Effect of Compatibilization on the Oxygen-Barrier Properties of Poly(ethylene terephthalate)/Poly(*m*-xylylene adipamide) Blends

V. Prattipati,[1] Y. S. Hu,[1] S. Bandi,[1] D. A. Schiraldi,[1] A. Hiltner,[1] E. Baer,[1] S. Mehta[2]

[1]*Department of Macromolecular Science and Center for Applied Polymer Research, Case Western Reserve University, Cleveland, Ohio 44106-7202*
[2]*Invista, 1551 Sha Lane, Spartanburg, South Carolina 29304*

Received 8 October 2004; accepted 28 December 2004
DOI 10.1002/app.21843
Published online in Wiley InterScience (www.interscience.wiley.com).

ABSTRACT: The improvement of the oxygen-barrier properties of poly(ethylene terephthalate) (PET) via blending with an aromatic polyamide [poly(*m*-xylylene adipamide) (MXD6)] was studied. The compatibilization of the blends was attempted through the incorporation of small amounts of sodium 5-sulfoisophthalate (SIPE) into the PET matrix. The possibility of a transamidation reaction between PET and MXD6 was eliminated by ^{13}C-NMR analysis of melt blends with 20 wt % MXD6. An examination of the blend morphology by atomic force microscopy revealed that SIPE effectively compatibilized the blends by reducing the MXD6 particle size. Thermal analysis showed that MXD6 had a nucleating effect on the crystallization of PET, whereas the crystallization of MXD6 was inhibited, especially in compatibilized blends. Blending 10 wt % MXD6 with PET had only a small effect on the oxygen permeability of the unoriented blend when it was measured at 43% relative humidity, as predicted by the Maxwell model. However, biaxially oriented films with 10 wt % MXD6 had significantly reduced oxygen permeability in comparison with PET. The permeability at 43% relative humidity was reduced by a factor of 3 in compatibilized blends. Biaxial orientation transformed spherical MXD6 domains into platelets oriented in the plane of the film. An enhanced barrier arose from the increased tortuosity of the diffusion pathway due to the high aspect ratio of MXD6 platelets. The aspect ratio was calculated from the macroscopic draw ratio and confirmed by atomic force microscopy. The reduction in permeability was satisfactorily described by the Nielsen model. The decrease in the oxygen permeability of biaxially oriented films was also achieved in bottle walls blown from blends of PET with MXD6. © 2005 Wiley Periodicals, Inc. J Appl Polym Sci 97: 1361–1370, 2005

Key words: blends; polyesters; gas permeation

INTRODUCTION

Blends of poly(ethylene terephthalate) (PET) and aromatic polyamides are of interest in the area of food packaging because of their potential for combining the low oxygen and carbon dioxide permeability of the polyamides with the good toughness, clarity, and economics of the polyester.[1] Although these blends suffer from low optical clarity and the generation of an undesirable yellow color during processing,[2] improved gas-barrier properties make the further investigation of PET/polyamide blends attractive.

Achieving the optimum barrier structure of PET/polyamide blends is compromised by the incompatibility of the constituent polymers. In several examples, small amounts of an ionomer have been added to compatibilize blends that incorporate a highly polar constituent. The ionic groups are presumed to interact with the polar constituent, whereas the nonionic backbone of the ionomer is compatible with the less polar constituent. Thus, otherwise incompatible polyethylene/polyamide blends have been made compatible by the addition of poly(ethylene-*co*-methacrylic acid) ionomers.[3,4]

Sulfonated ionomers are known to interact strongly with aliphatic polyamides,[5] establishing a network structure in which sulfonate anions coordinate to amide N—H groups, whereas the counterions complex to multiple amide carbonyl oxygen groups.[6] The use of sulfonated polyester ionomers as compatibilizers for PET and aliphatic polyamides has been demonstrated, with both ion–dipole interaction and transesterification reactions thought to play a role in compatibilization.[7–9] Given these precedents, it seems reasonable that polyester ionomers would also compatibilize blends of PET with aromatic polyamides.

This study examines the morphology and oxygen-barrier properties of PET blended with an aromatic polyamide. Compatibilization by the incorporation of sulfonated groups into the PET matrix has been attempted. The findings on biaxially oriented films are compared with results for blown bottle walls.

Correspondence to: A. Hiltner (pah6@cwru.edu).
Contract grant sponsor: Invista.

EXPERIMENTAL

PET and a copolymer based on PET with 2.29 mol % terephthalate replaced with sodium 5-sulfoisophthalate (PET-*co*-SIPE) were provided by Invista (Spartanburg, SC) in the form of extruded pellets. The intrinsic viscosities of PET and PET-*co*-SIPE were 0.84 and 0.56 dL g^{-1}, respectively, at 25°C in a dichloroacetic acid solution. Poly(*m*-xylylene adipamide) (MXD6) pellets with a number-average molecular weight of 16,500 (grade 6001) were obtained from Mitsubishi Gas Chemical America, Inc (New York, NY).

PET and MXD6 were dried at 120°C for 48 h *in vacuo*, and PET-*co*-SIPE was dried at 80°C *in vacuo*. Pellets of PET, PET-*co*-SIPE, and MXD6 were dry-mixed to produce blends with 10 wt % MXD6, unless indicated otherwise, and various amounts of sodium 5-sulfoisophthalate (SIPE). The dry blends were extruded in a Daca twin-screw extruder (Goleta, CA) with partially corotating and self-wiping conical screws. The screw had a diameter of 13.75 mm and was 108 mm long. A barrel temperature of 270°C and a screw speed of 100 rpm were used for these extrusions. Good dispersion is favored for a low-viscosity minor constituent in a more viscous matrix.[10] The lower viscosity of MXD6, compared with that of PET, at the blending temperature of 270°C, as indicated by melt-flow-index measurements, promoted the dispersion of the MXD6 phase. A residence time of approximately 2 min was used for each 4-g batch. The molten blend was extruded through a 2-mm die and pelletized. The PET, PET-*co*-SIPE, and MXD6 controls were also extruded, as described previously. Transesterification during melt blending completely randomized PET and PET-*co*-SIPE to produce a homogeneous matrix copolymer. The blends are designated as wt % matrix (mol % SIPE in the matrix)/wt % MXD6.

Pellets of extruded controls and blends were dried *in vacuo* at 80°C for 24 h before being molded into films. The dried pellets were compression-molded between Kapton films and quenched into ice water, as described previously.[11] The temperature of the press was 270°C. Films approximately 200 μm thick were prepared in this manner.

Compression-molded films were analyzed for possible transamidation between PET and MXD6 by means of ^{13}C-NMR with a Varian Gemini 2000 300-MHz FT-NMR spectrometer (Palo Alto, CA). Blends with 20 wt % MXD6 were used to increase the signal level. Films of PET and 80(0.00)/20 and 80(2.29)/20 blends were dissolved in a 4:1 (v/v) solution of *d*-trifluoroacetic acid (TFA) and *d*-chloroform ($CDCl_3$) at room temperature, whereas the MXD6 film was dissolved in neat TFA. The NMR spectra were run at the ambient temperature.

The blend morphology was examined with atomic force microscopy (AFM) with the Nanoscope IIIa MultiMode head from Digital Instruments (Santa Barbara, CA) in the tapping mode. Specimens were microtomed at the ambient temperature to expose the bulk morphology. Phase and height images were recorded simultaneously.

Films of PET and the blends were dried at 70°C, and MXD6 was dried at 80°C for 2 days to obtain the dry thermograms. Thermal analysis was conducted with a PerkinElmer Pyris-1 (Boston, MA). The heating scan was performed at 10°C min^{-1} from 30 to 270°C. After 5 min at 270°C, the cooling scan was obtained at the same rate.

Dog-bone-shaped specimens (type I, ASTM D 638) were cut from the compression-molded films and were conditioned at 43% relative humidity (RH) before the drawing. Uniaxial tensile tests were conducted at the ambient temperature and RH on an Instron 1123 mechanical testing machine (Canton, MA) with a strain rate of 50% min^{-1}.

For the barrier measurements, some of the blend compositions were scaled up in a Haake Rheomex TW-100 (Karlsruhe, Germany) continuous twin-screw extruder with partially intermeshing, counter-rotating, conical screws with converging axes. The average screw diameter was 25.4 mm, and the average length/diameter ratio was 13/1. A barrel temperature of 285°C and a screw speed of 15 rpm were used. The molten blends were extruded through a 3-mm die and pelletized. Films approximately 200 or 600 μm thick were compression-molded, as described earlier. The 200-μm-thick films were used for testing the oxygen barrier.

The 600-μm films were biaxially oriented. The films were conditioned at 43% RH, which dropped the glass-transition temperature (T_g) of MXD6 from 84 to 48°C. The lower T_g facilitated the orientation of the MXD6 domains. The conditioned film with a gauge section 15 cm wide and 4 cm long was mounted in the environmental chamber of an Instron machine. The film was stretched uniaxially at 75°C to a draw ratio of 4, remounted in the grips at 90°C to the first stretch, and stretched again at 78°C to achieve a final balanced biaxial draw ratio of 2.7 $\times$ 2.7. Stretching was performed at a rate of 20% min^{-1}. Grids were marked on the specimen for measuring the draw ratio. After the drawing, the film was rapidly cooled to the ambient temperature.

Two-liter carbonated-soft-drink bottles made from PET and PET blends were supplied by Invista. The bottles were blown from preforms with a commercial blow-molding machine (Sidel, Norcross, GA) after the bottle performs were conditioned at 54% RH. The side-wall temperatures were nominally 90°C. The blowing cycle time was 3 s. The bottle-wall draw ratio of 2.5 $\times$ 4.0 (axial$\times$hoop) was typical of commercial bottle production. The wall section was cut from the bottle for subsequent characterization.

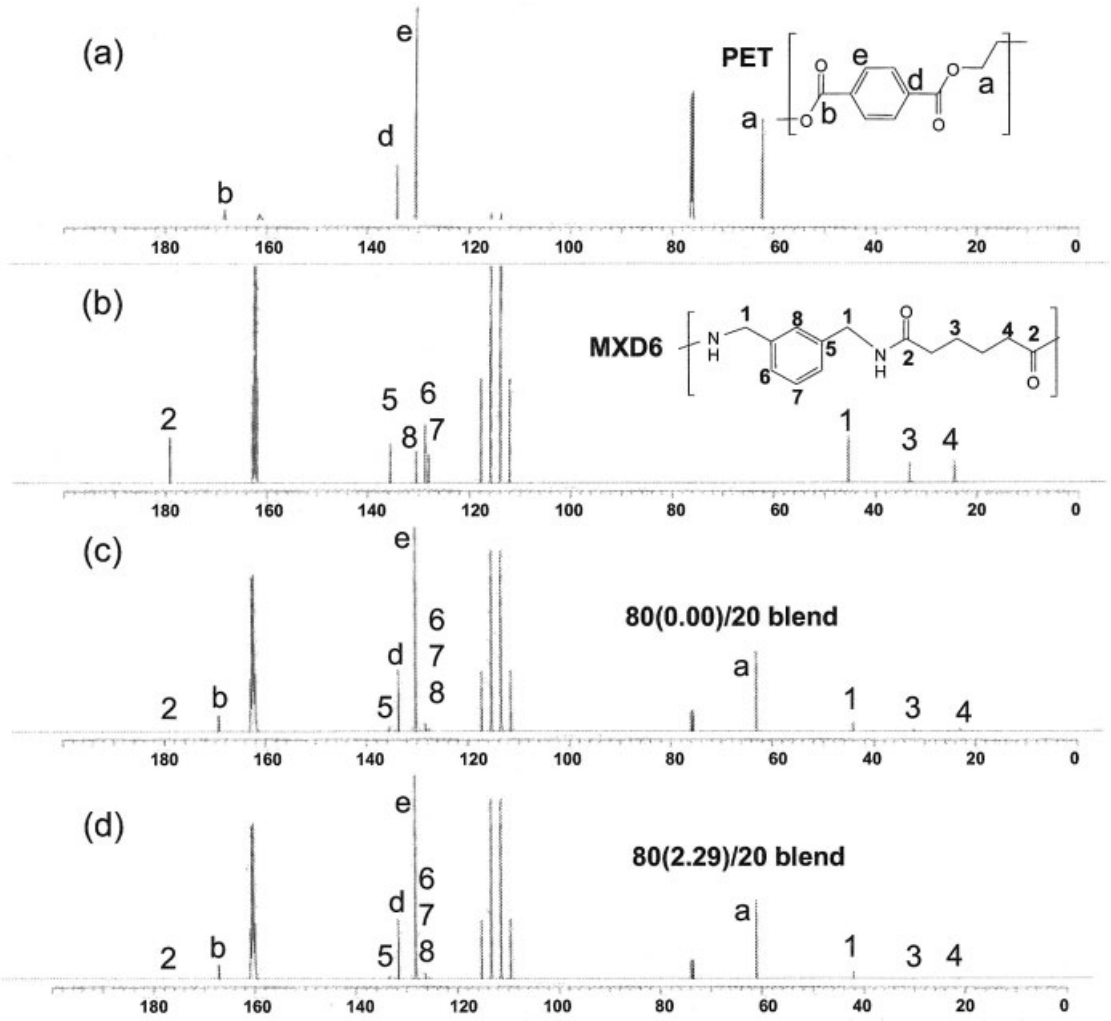

Figure 1 ^{13}C-NMR spectra of (a) PET, (b) MXD6, (c) an 80(0.00)/20 blend, and (d) an 80(2.29)/20 blend.

Oxygen flux $J(t)$ at 23°C, 43% RH, and 1 atm of pressure was measured with a Mocon Ox-Tran 2/20 (Minneapolis, MN). The instrument was calibrated with National Institute of Standards and Technology certified Mylar film of known oxygen-transport characteristics. Samples were equilibrated at 43% RH before the barrier was tested. Specimens were carefully conditioned, as described previously,[11] to obtain the non-steady-state $J(t)$ values. To obtain diffusivity D and to accurately determine permeability P, the data were fit to the solution of Fick's second law with appropriate boundary conditions:

$$J(t) = \frac{Pp}{l}\left[1 + 2\sum_{n=1}^{\infty}(-1)^n \exp\left(-\frac{D\pi^2 n^2 t}{l^2}\right)\right] \quad (1)$$

where p is the pressure, t is the time, and n is an integer. The thickness l was determined from the measured density, as described previously,[11] after the barrier measurement was completed.

RESULTS AND DISCUSSION

Characterization of the unoriented blends

The ^{13}C-NMR spectra of PET, MXD6, and 80(0.00)/20 and 80(2.29)/20 blends with their peak assignments are shown in Figure 1. The PET chains can terminate in either carboxylic acid or hydroxyl end groups, whereas MXD6 end groups can be either amines or carboxylic acids. During the melt blending of PET and MXD6, transamidation reactions are possible between PET carboxylic acid end groups and the amine end groups of MXD6. This polyamide formation would change the environment of the benzylic carbon of MXD6 and carbonyl carbon of PET; a new benzylic peak would be expected downfield of the existing benzylic peak (at 45.7 ppm) in the event of transamidation. Similarly, a new amide carbonyl signal would be expected downfield in the vicinity of the PET carbonyl peak (at 171.2 ppm). No new benzylic or carbonyl peaks were observed in the NMR spectra of the 80(0.00)/20 and 80(2.29)/20 blends [Fig. 1(c,d)]; this

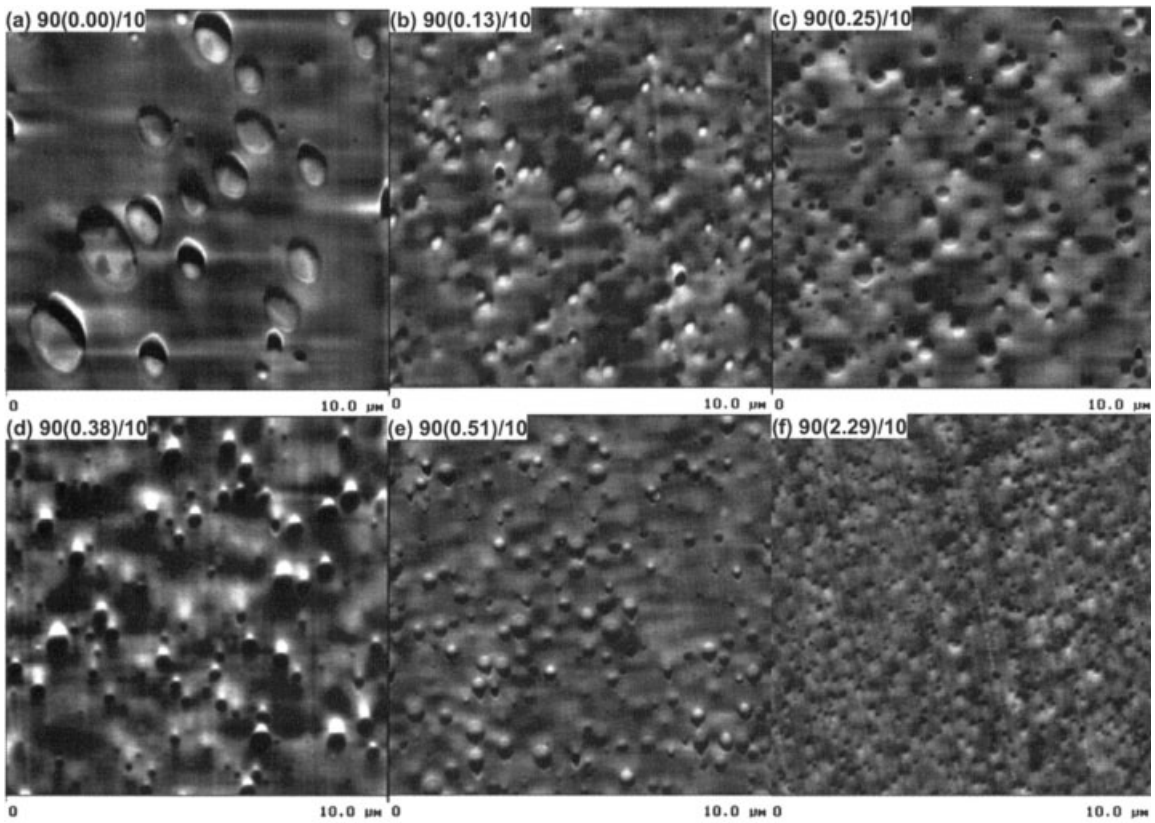

Figure 2 AFM height images of unoriented blends: (a) 90(0.00)/10, (b) 90(0.13)/10, (c) 90(0.25)/10, (d) 90(0.38)/10, (e) 90(0.51)/10, and (f) 90(2.29)/10.

indicates that there is no significant transamidation between PET and MXD6 under the processing conditions employed in this study.

The morphology of blends with various amounts of SIPE is shown in Figure 2. The blends had spherical or slightly ellipsoidal MXD6 particles dispersed in the continuous PET matrix. A 10-μm AFM height image of the 90(0.00)/10 blend showed MXD6 domains ranging from 0.2 to 2.0 μm in diameter [Fig. 2(a)]. The incorporation of SIPE into the PET matrix reduced the domain size of 90(0.13)/10 to approximately 0.1–0.7 μm [Fig. 2(b)]. The domain size decreased somewhat further with an increasing amount of SIPE to about 0.1–0.2 μm for 90(2.29)/10. Thus, the incorporation of SIPE into the PET matrix effectively compatibilized the blends by reducing the particle size.

The first heating and subsequent cooling thermograms of dry films are shown in Figure 3. The corresponding T_g's, peak crystallization temperatures, and peak melting temperatures (T_m's) and their enthalpies are given in Table I. PET had T_g at 78°C, a peak cold crystallization temperature (T_{cc}) at 139°C, and T_m at 247°C. MXD6 had T_g at 84°C, T_{cc} at 129°C, and T_m at 234°C. In addition, MXD6 exhibited a second small cold crystallization peak immediately before the melting endotherm. Only a single T_g corresponding to that of PET was evident in the heating scans of the blends

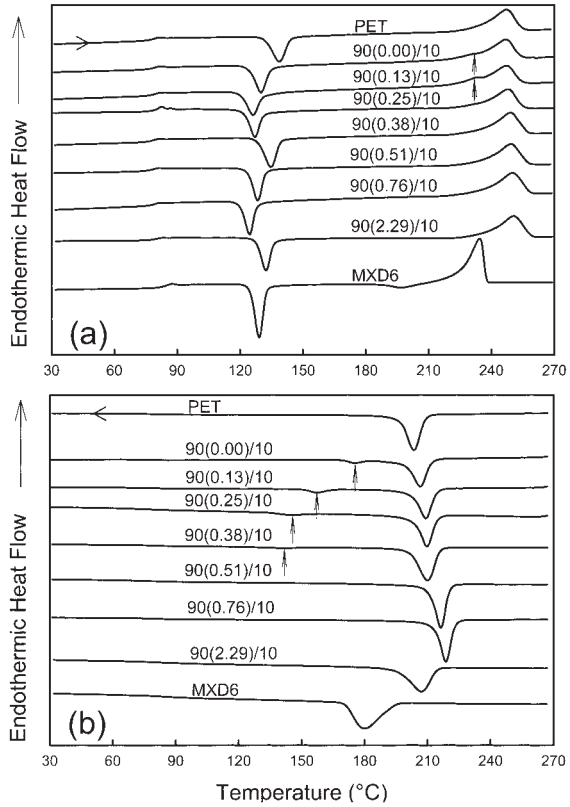

Figure 3 DSC thermograms of dry blends: (a) first heating and (b) subsequent cooling.

TABLE I
Thermal Analysis of Dry Blends

Composition	T_g (°C)	T_{cc} (°C)	ΔH_{cc} (J/g)	T_m (°C)	ΔH_m (J/g)	T_c (°C)	ΔH_c (J/g)
PET	78	139	34	247	40	203	43
90(0.00)/10	78	132	32	234,246	40	206,175	42,4
90(0.13)/10	78	126	32	233,247	41	209,157	42,3
90(0.25)/10	78	127	33	248	39	210,145	42,2
90(0.38)/10	77	135	32	249	43	210,140	44,2
90(0.51)/10	78	128	31	249	42	216	44
90(0.76)/10	79	125	30	250	44	219	44
90(2.29)/10	79	132	30	251	43	207	44
MXD6	84	129,200	40,7	234	55	180	56

ΔH_{cc} is the heat of cold crystallization, ΔH_m is the heat of melting, ΔH_c is the heat of melt crystallization.

because of the low content of MXD6 as well as the relatively small difference between the T_g's of PET and MXD6.

As is often the case when a second phase is added to PET,[12–15] MXD6 domains nucleated the cold crystallization of PET, as indicated by a shift in T_{cc} to a slightly lower temperature. Some scatter in T_{cc} among the various blends suggested that small differences in the thermal history affected cold crystallization; in this case, the differences probably occurred through small variations in the quenching time of the compression-molded films. A small endotherm in heating thermograms of the 90(0.00)/10 and 90(0.13)/10 blends at 234°C corresponded to T_m of MXD6. The small crystallization endotherm of MXD6 was not present in thermograms of blends with higher SIPE contents.

Cooling thermograms clearly showed the nucleating effect of melted MXD6 particles on the crystallization of PET from the melt. The peak melt crystallization temperature (T_c) of PET gradually shifted to higher temperature as the SIPE content increased. However, increasing the SIPE content further, from the 90(0.76)/10 blend to the 90(2.29)/10 blend, reversed the trend and resulted in T_c close to that of 90(0.00)/10. A crystallization peak for MXD6 could be observed clearly in the cooling scan of blends with lower amounts of SIPE. T_c of MXD6 particles gradually shifted to a lower temperature and the crystallization enthalpy decreased with an increasing amount of SIPE until the peak was no longer evident in the cooling thermogram of 90(0.51)/10 and blends with higher SIPE contents.

It is often observed that if the minor phase of an immiscible blend is highly dispersed, it crystallizes at a supercooling higher than that required normally.[16–19] This is attributed to the number of droplets being significantly higher than the number of active heterogeneities present at a low supercooling. Hence, only those droplets that contain the heterogeneities crystallize at the normal temperature. Other droplets containing less active heterogeneities crystallize at a higher supercooling, and finally those droplets that do not contain any heterogeneity crystallize by homogeneous nucleation at the largest supercooling. This is called fractionated crystallization.

On the basis of the average particle sizes of 0.175, 0.160, and 0.130 μm for the 90(0.13)/10, 90(0.25)/10, and 90(0.51)/10 blends, the number of MXD6 droplets was calculated to be 4.5×10^{12}, 5.8×10^{12}, and 1.1×10^{13} per cubic centimeter, respectively. The reported nucleation densities of PET,[17] polypropylene,[18] and high-density polyethylene[18] are 3×10^6, 9×10^6, and 1×10^9 per cubic centimeter, respectively. If MXD6 has a number of heterogeneities similar to that reported for other polymers, the number of dispersed particles is orders of magnitude higher than the number of heterogeneities. The melt crystallization temperature of MXD6 shifts because of less active heterogeneities, which nucleate crystallization at a higher supercooling. An increase in the supercooling has been reported of as much as 50°C for polyethylene droplets in polystyrene and of as much as 70°C for nylon 6 in polypropylene.[20] Possibly the supercooling required for the crystallization of MXD6 droplets brings T_c close enough to T_g that crystallization is not realized because of a lack of sufficient chain mobility. However, fractionated crystallization alone does not account for the effect of SIPE on MXD6 droplet crystallization. The number of droplets does not change significantly between the 90(0.13)/10 and 90(0.51)/10 blends, although MXD6 droplets crystallize in the former but not in the latter. This implies that in addition to the small particle size, strong interactions between SIPE and MXD6 retard crystallization. Similar behavior has been reported for nylon 6 compatibilized with maleated polypropylene (PP-*g*-MA).[20]

Specimens conditioned at 43% RH were used for tensile testing. The stress–strain curves of PET and the blends are shown in Figure 4, and the corresponding tensile properties are given in Table II. The yielding of PET was followed by neck propagation along the gauge section to about 200% strain and by uniform strain hardening with strain-induced crystallization at higher strain until fracture. In contrast, MXD6 condi-

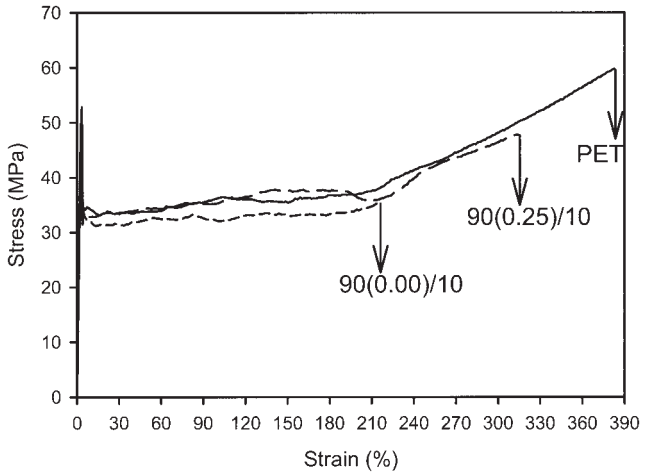

Figure 4 Engineering stress–strain curves of PET and 90(0.00)/10 and 90(0.25)/10 blends.

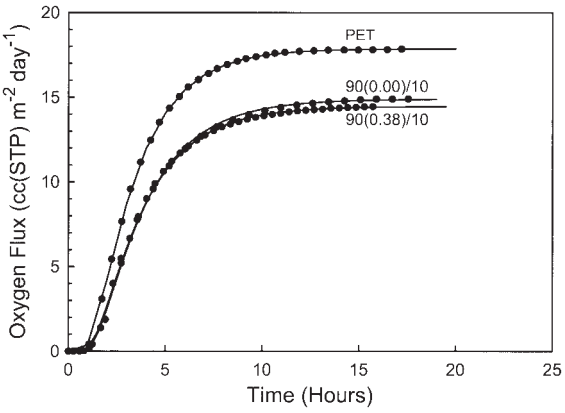

Figure 5 $J(t)$ curves of unoriented PET and 90(0.00)/10 and 90(0.38)/10 blends tested at 43% RH.

tioned at 43% RH fractured without yielding at about 3.3% strain, which was only a slight improvement over the 2.3% fracture strain reported for the dry sample.[21] The uncompatibilized blend had lower yield stress than PET, and this indicated that the interface failed before the stress reached the yield stress of PET. The subsequent formation and growth of voids resulted in stress whitening during neck propagation in the 90(0.00)/10 blend. On the other hand, the compatibilized blend had yield stress identical to that of PET. Better adhesion in the 90(0.25)/10 blend prevented interfacial failure before global yielding. In the absence of debonding and void formation, the neck propagated without apparent stress whitening. Compatibilization also affected fracture behavior. Whereas the 90(0.00)/10 blend fractured at the end of the neck propagation region, the 90(0.25)/10 blend underwent significant strain hardening before fracture. Better adhesion and smaller particle size in the compatibilized blend improved ductility by retarding the formation of a critical size flaw.

Oxygen barrier of the unoriented blends

Typical experimental curves in Figure 5 describe $J(t)$ through unoriented PET and 90(0.00)/10 and 90(0.38)/10 blends tested at 23°C and 43% RH. The flux curves were normalized to a film thickness of 200 μm to facilitate comparisons among specimens that varied slightly in thickness. Careful conditioning and the appropriate choice of the specimen thickness resulted in excellent resolution of the various features of the time dependence. The initial increase in $J(t)$ reflected non-steady-state diffusion. This part of the curve was controlled mainly by D. As the permeant concentration in the specimen reached a constant distribution, the flux reached the steady-state value, J_0. This value, normalized to the film thickness l and the permeant gas pressure p, defined $P = J_0 l p^{-1}$.

The fit to the solution of Fick's second law [eq. (1)] is included with the experimental points in Figure 5. The fit was equally good for all the experiments in the study. The two fitting parameters, P/l and D/l^2, were used to obtain D and to accurately determine P. Solubility S was calculated with the relationship $S = PD^{-1}$. The non-steady-state region broadened (slower diffusion) and the steady-state flux decreased (lower P) slightly for the blends in comparison with PET.

The oxygen-barrier properties tested at 43% RH for the unoriented PET, MXD6, and blend films with 10 wt % MXD6 and various amounts of SIPE are shown in Table III. The permeability of MXD6 (P_{MXD6}) was considerably lower than the permeability of PET (P_{PET}) by a factor of 0.02, which was mainly due to lower D. Blending with 10 wt % MXD6 reduced P_{PET} slightly to a P/P_{PET} value of about 0.82, which was due to lower D. Compatibilization did not affect the barrier of the unoriented blends. Oxygen solubility should depend only on the blend composition and, at equilibrium, should be equal to the additive contributions of the blend constituents based on the volume fraction. For blends with 10 wt % (11 vol %) MXD6, S was calculated to be 0.074 cc (STP) cm^{-3} atm^{-1}, in good agreement with the experimental results. D and

TABLE II
Tensile Properties of Blends Conditioned at 43% RH

Composition	Yield stress (MPa)	Yield strain (%)	Fracture stress (MPa)	Fracture strain (%)
PET	53 ± 1	3.8 ± 0.4	60 ± 4	386 ± 25
90(0.00)/10	49 ± 1	3.3 ± 0.3	39 ± 6	239 ± 33
90(0.25)/10	53 ± 3	3.4 ± 0.1	43 ± 6	263 ± 47
MXD6	—	—	58 ± 11	3.3 ± 0.4

TABLE III
Oxygen-Barrier Properties of Unoriented Blends Tested at 43% RH

Composition	Density (g cm^3)	P	D	S	P/P_{PET}
PET	1.3379	0.363	5.2	0.081	1.00
90(0.00)/10	1.3256	0.303	4.5	0.078	0.83
90(0.38)/10	1.3258	0.295	4.6	0.074	0.81
90(0.76)/10	1.3266	0.298	4.4	0.078	0.82
MXD6	1.2050	0.0067	0.40	0.019	0.02

P [cc (STP) cm m^{-2} atm^{-1} day^{-1}]; D (10^{-13} m^2/s); S [cc (STP) cm^{-3} atm^{-1}].

hence P depend on the blend morphology as well as the blend composition. Consequently, models for the gas permeability of polymer blends must consider the shape and spatial orientation of the dispersed phase.

The permeability of blends consisting of less permeable spherical particles dispersed in a more permeable matrix can be predicted by the Maxwell model as follows:[22]

$$\frac{P}{P_{PET}} = 1 + \frac{3\phi_{MXD6}}{\dfrac{(P_{MXD6}/P_{PET})+2}{(P_{MXD6}/P_{PET})-1} - \phi_{MXD6}} \quad (2)$$

For blends with 10 wt % MXD6, the volume fraction is calculated as $\phi_{MXD6} = 0.11$ with the measured densities of PET and MXD6. From the measured values of P_{PET} and P_{MXD6}, eq. (2) gives $P/P_{PET} = 0.85$, which is in good agreement with the experimental result of approximately 0.82 (Table III).

Biaxially oriented blends

Films were conditioned at 43% RH and sequentially oriented to a draw ratio of 2.7 × 2.7. The AFM phase images of cross sections from biaxially oriented 90(0.00)/10 and 90(0.38)/10 films showed the platelet shape of the MXD6 phase (Fig. 6). A large variation in the particle size of 90(0.00)/10 resulted in platelets that varied from 2 to 6 μm in length and from 90 to 500 nm in thickness. The larger platelets had an aspect ratio (length-to-thickness ratio) as low as 15. For 90(0.38)/10, the average platelet length and thickness were about 1.0–1.8 μm and 35 nm, respectively, which gave an aspect ratio of 28.

Biaxial orientation reduced P_{PET} from 0.363 to 0.253 cc (STP) cm m^{-2} atm^{-1} day^{-1} as a result of decreases in both D and S (Tables III and IV). The decrease in S and the corresponding increase in the density that accompany the orientation of glassy PET have been identified with the loss of free volume.[23] In contrast, biaxial orientation increased P_{MXD6} from 0.007 to 0.011 cc (STP) cm m^{-2} atm^{-1} day^{-1} as a result of increases in both D and S (Tables III and IV). The density decreased correspondingly. Apparently, hydrogen bonds in the aromatic polyamide inhibited the conformational changes that would have reduced the free volume and, therefore, reduced permeability, as in oriented PET. Instead, partial disruption of the hydrogen bonding resulted in dedensification and increased oxygen permeability.[24]

The effect of blending is shown in Figure 7 through a comparison of $J(t)$ through biaxially oriented PET and 90(0.00)/10 and 90(0.38)/10 films tested at 23°C and 43% RH with the flux normalized to a film thickness of 200 μm. Blending with MXD6 significantly broadened the non-steady-state region (slower diffusion) and decreased the steady-state flux (lower permeability). The platelet morphology of the less permeable dispersed phase significantly reduced the gas permeability in comparison with the spherical droplet morphology in unoriented blends (cf. Fig. 7 with Fig. 5).

The effect of SIPE on the oxygen-barrier properties of biaxially oriented blends with 10 wt % MXD6 tested at 43% RH is shown in Table IV. A small amount of

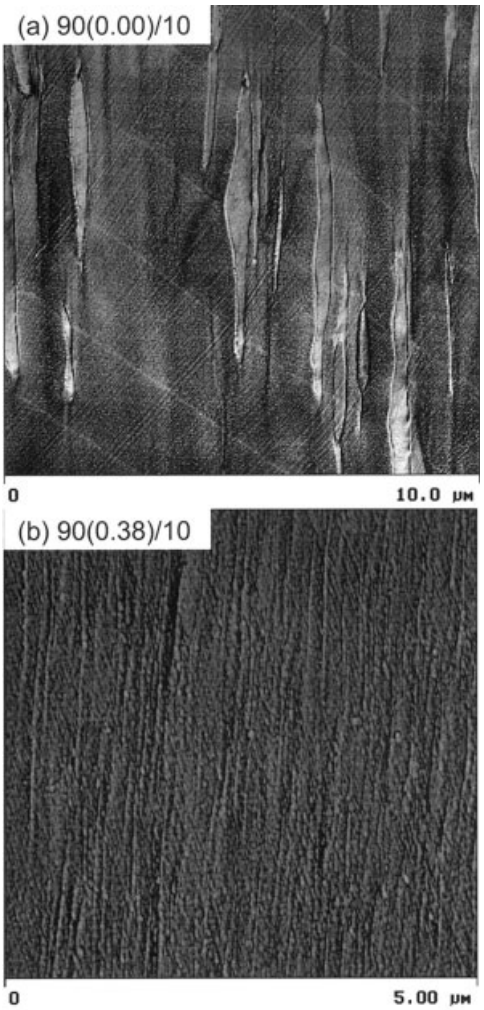

Figure 6 AFM phase images of biaxially oriented blends: (a) 90(0.00)/10 and (b) 90(0.38)/10.

TABLE IV
Oxygen-Barrier Properties of Biaxially Oriented Blends Tested at 43% RH

Composition	Density (g/cm^3)	P	D	S	P/P_{PET}	Aspect ratio [eq. (3)]
PET	1.3544	0.253	4.3	0.068	1.00	—
90(0.00)/10	1.3312	0.135	2.3	0.068	0.53	12
90(0.38)/10	1.3406	0.078	1.5	0.060	0.31	34
90(0.76)/10	1.3398	0.080	1.6	0.058	0.32	32
90(1.52)/10	1.3404	0.111	2.1	0.061	0.44	18
90(2.29)/10	1.3412	0.107	2.1	0.059	0.42	20
MXD6	1.2034	0.011	0.46	0.028	0.04	—

P [cc (STP) cm m^{-2} atm^{-1} day^{-1}]; D (10^{-13} m^2/s); S [cc (STP) cm^{-3} atm^{-1}].

SIPE in the blend decreased P in comparison with P of the uncompatibilized blend because of lower D and S. Lower D suggested that better adhesion and smaller particle size in the compatibilized blends facilitated deformation of the MXD6 domains into platelets of higher aspect ratio, thereby imparting greater tortuosity to the diffusion pathway. The oxygen solubility of the compatibilized blend was close to the additive value. Perhaps S of the blend without SIPE exceeded the additive value because of debonding at the poorly adhered interface. Surprisingly, a higher SIPE content resulted in increased P; this was caused by an increase in D. It is possible that as the particles became smaller and better adhered to the matrix, they oriented less readily or were too thin after orientation to retain good barrier properties.

The biaxially oriented blends closely resemble the structure modeled by Nielsen,[25] in which impermeable platelets of a given aspect ratio are dispersed in a permeable matrix with the platelets oriented perpendicularly to the gas flow. Although orientation brings the oxygen permeabilities of PET and MXD6 somewhat closer together, P of MXD6 remains much lower than P of PET (Table IV), and the MXD6 platelets can be considered impermeable in accordance with the model. The Nielsen model relates the reduction in permeability to the platelet aspect ratio as follows:

$$\frac{P}{P_{PET}} = \frac{1 - \phi_{MXD6}}{1 + \frac{\alpha}{2}\phi_{MXD6}} \quad (3)$$

where α is the aspect ratio of the platelets. The aspect ratio of 34 obtained from eq. (3) for compatibilized blends agreed well with the value estimated from the AFM image of film cross sections.

The maximum aspect ratio that can be achieved for the MXD6 domains is determined by the biaxial draw ratio of 2.7 × 2.7. Assuming that spherical domains deform affinely into circular disks, a simple calculation based on volume conservation gives

$$\frac{4}{3}\pi r^3 = \pi(\lambda r)^2 W \Rightarrow \alpha = \frac{L}{W} = \frac{2\lambda r}{W} = \frac{3}{2}\lambda^3 \quad (4)$$

where r is the radius of the spherical domains; λ is the balanced biaxial draw ratio; and L and W are the length and thickness of the circular disk, respectively. From eq. (4), the maximum aspect ratio for these platelets is 30, which is in good agreement with the experimental observation from AFM and the result from the Nielsen model based on permeability.

Even lower permeability can be achieved with the blends if the particle aspect ratio is increased in accordance with eq. (3). A lower bound on P for a given blend composition can be obtained by the consideration of a series arrangement of infinite PET and MXD6 layers:

$$\frac{1}{P} = \frac{1 - \phi_{MXD6}}{P_{PET}} + \frac{\phi_{MXD6}}{P_{MXD6}} \quad (5)$$

The minimum P/P_{PET} value for a PET blend with 10 wt % (11 vol %) MXD6, as given by eq. (5), is 0.29. For comparison, values as low as 0.31 were achieved with 2.7 × 2.7 biaxial orientation, which was very close to the maximum barrier improvement.

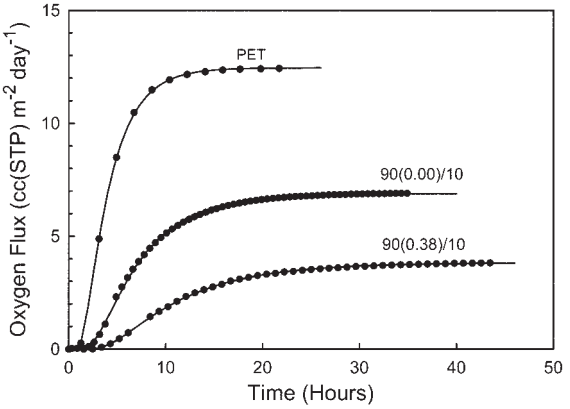

Figure 7 $J(t)$ curves of biaxially oriented PET and 90(0.00)/10 and 90(0.25)/10 blends tested at 43% RH.

TABLE V
Oxygen-Barrier Properties of Blend Bottle Walls Tested at 43% RH

Composition	Density (g/cm^3)	P	D	S	P/P_{PET}	Aspect ratio [eq. (3)]
PET	1.3667	0.195	3.4	0.066	1.00	—
90(0.00)/10	1.3499	0.077	1.4	0.064	0.39	22
90(0.38)/10	1.3523	0.055	1.0	0.064	0.28	38

P [cc(STP) cm m^{-2} atm^{-1} day^{-1}]; D (10^{-13} m^2/s); S [cc (STP) cm^{-3} atm^{-1}].

Blown bottle walls

Concepts developed for biaxially oriented films were extended to the blown bottle wall. Tested at 43% RH, the PET bottle wall showed lower permeability than the biaxially oriented film because of the faster draw rate in the bottle-blowing process. The bottle wall blown from the uncompatibilized blend with 10 wt % MXD6 had $P/P_{PET} = 0.39$ (Table V). Compatibilization resulted in a lower P/P_{PET} value of 0.28. Although the absolute values of P were always lower for the bottle wall than for the biaxially oriented film, the reduction in P of the blend with respect to P_{PET} closely paralleled the result predicted by 2.7 × 2.7 biaxial orientation, especially for the compatibilized blend.

The aspect ratio of the MXD6 domains calculated from eq. (3) was 22 and 38 in the 90(0.00)/10 and 90(0.38)/10 blend bottle walls, respectively. The draw ratio in the bottle wall, as determined from the dimensions of the preform and bottle, was 4.0 (hoop) ×2.5 (axial). Unbalanced biaxial orientation produced MXD6 platelets with an elliptical shape. From volume conservation and the draw ratio, the maximum aspect ratio based on the shorter dimension of the ellipse was 38, which agreed with the result from eq. (3) for the compatibilized blend. It appears that biaxially oriented films reliably predict the relative decrease in permeability that can be achieved in PET bottle walls through blending with a low-permeability constituent.

CONCLUSIONS

This study demonstrates how the oxygen barrier of PET can be dramatically improved via blending with a high-barrier constituent, in this case with 10 wt % of an aromatic polyamide. Incorporating a small amount of SIPE into the PET matrix effectively compatibilized the blends by reducing the polyamide domain size. Compatibilization also inhibited crystallization of the polyamide. However, the polyamide nucleated crystallization of PET by reducing the cold crystallization temperature and increasing the crystallization temperature from the melt.

Blending 10 wt % MXD6 with PET had only a small effect on the oxygen permeability of the unoriented blend when it was measured at 43% RH, as predicted by the Maxwell model. However, biaxial orientation of the blend transformed spherical polyamide domains into platelets of high aspect ratio arrayed in the plane of the film. The oxygen permeability was reduced by as much as a factor of 3 because of the increased tortuosity of the diffusion pathway. Polyamide domains in compatibilized blends achieved the maximum aspect ratio of about 30 on the basis of the draw ratio of 2.7 × 2.7. This was predicted by an analysis of the oxygen permeability according to the Nielsen model and was confirmed experimentally by AFM. The polyamide domains in uncompatibilized blends did not achieve the maximum draw ratio during biaxial orientation, and so the oxygen permeability was not reduced to the same extent as in compatibilized blends.

The results observed with balanced biaxially oriented films were reproduced in blown bottle walls. Although the bottle was blown under different conditions of the temperature and rate to an unbalanced biaxial draw ratio, the reduction in oxygen permeability achieved with 10 wt % polyamide was the same as that in the films. The correspondence extended to the effect of the compatibilizer. This finding makes it possible to use oriented films as a model system for optimizing the gas barrier of the blown bottle.

Modern Controls, Inc., generously supported the development of a facility for gas-transport studies at Case Western Reserve University.

References

1. Akkapeddi, M. K.; Kraft, T. J.; Socci, E. P. U.S. Pat. 6,685,861 (2004).
2. Bell, E. T.; Bradley, J. R.; Long, T. E.; Stafford, S. L. U.S. Pat. 6,239,233 (2001).
3. Sheng, J.; Ma, H.; Yuan, X.-B.; Yuan, X.-Y.; Shen, N.-X.; Bian, D.-C. J Appl Polym Sci 2000, 76, 488.
4. Leewajanakul, P.; Pattanaolarn, R.; Ellis, J. W.; Nithitanakul, M.; Grady, B. P. J Appl Polym Sci 2003, 89, 620.
5. Eisenberg, A.; Kim, J.-S. Introduction to Ionomers; Wiley: New York, 1998; Chapter 9, p 267.
6. Rajagopalan, P.; Lim, J.-S.; Brack, H. P.; Lu, X.; Eisenberg, A.; Weiss, R. A.; Risen, W. M., Jr. J Polym Sci Part B: Polym Phys 1995, 33, 495.
7. Boykin, T. L.; Moore, R. B. Polym Eng Sci 1998, 38, 1658.
8. Samios, C. K.; Kalfoglou, N. K. Polymer 1999, 40, 4811.
9. Zheng, X. J.; Zhang, J.; He, J. S. J Appl Polym Sci 2003, 87, 1452.
10. Wu, S. H. Polym Eng Sci 1987, 27, 335.

11. Sekelik, D. J.; Stepanov, E. V.; Nazarenko, S.; Schiraldi, D.; Hiltner, A.; Baer, E. J Polym Sci Part B: Polym Phys 1999, 37, 847.
12. Kamal, M. R.; Sahto, M. A.; Utracki, L. A. Polym Eng Sci 1982, 22, 1127.
13. Varma, D. S.; Dhar, V. K. J Appl Polym Sci 1987, 33, 1103.
14. Nadkarni, V. M.; Shingankuli, V. L.; Jog, J. P. Polym Eng Sci 1988, 28, 1326.
15. Tanrattanakul, V.; Hiltner, A.; Baer, E.; Perkins; W. G.; Massey, F. L.; Moet, A. Polymer 1997, 38, 2191.
16. Arnal, M. L.; Matos, M. E.; Morales, R. A.; Santana, O. O.; Muller, A. J. Macromol Chem Phys 1998, 199, 2275.
17. Molinuevo, C. H.; Mendez, G. A.; Muller, A. J. J Appl Polym Sci 1998, 70, 1725.
18. Arnal, M. L.; Muller, A. J. Macromol Chem Phys 1999, 200, 2559.
19. Manaure, A. C.; Muller, A. J. Macromol Chem Phys 2000, 201, 958.
20. Moon, H.-S.; Ryoo, B.-K.; Park, J.-K. J Polym Sci Part B: Polym Phys 1994, 32, 1427.
21. Nylon-MXD6 Product Bulletin; Mitsubishi Gas Chemical: New York, 2002.
22. Petropoulos, J. H. Adv Polym Sci 1985, 64, 93.
23. Liu, R. Y. F.; Schiraldi, D. A.; Hiltner, A.; Baer, E. J Polym Sci Part B: Polym Phys 2002, 40, 862.
24. Backman, A.; Lange, J.; Hedenqvist, M. S. J Polym Sci Part B: Polym Phys 2004, 42, 947.
25. Nielsen, L. E. J Macromol Sci Chem 1967, 1, 929.